Int J Adv Manuf Technol (2014) 72:69–75
DOI 10.1007/s00170-014-5656-3

ORIGINAL ARTICLE

A comparison between conventional speed grinding and super-high speed grinding of (TiC_p+TiB_w)/Ti–6Al–4V composites using vitrified CBN wheel

B. Zhao · W. F. Ding · J. B. Dai · X. X. Xi · J. H. Xu

Received: 8 October 2013 / Accepted: 20 January 2014 / Published online: 7 February 2014

Abstract Comparative grinding experiments of (TiC_p+TiB_w)/Ti–6Al–4V composites were conducted using vitrified CBN wheel at the conventional wheel speed of 20 m/s and the super-high wheel speed of 120 m/s, respectively. The grinding behavior, i.e., grinding force and force ratio, grinding temperature, specific grinding energy, and ground surface morphology were analyzed. The results obtained indicate that the normal and tangential grinding forces at the super-high wheel speed are smaller than that at the conventional wheel speed. However, the force ratio, the specific grinding energy, and the grinding temperature show a contradictory trend compared to the grinding force between the conventional speed grinding and the super-high speed grinding. The main defects of the ground surface of (TiC_p+TiB_w)/Ti–6Al–4V composites are voids, micro-cracks, fracture or crushed, pulled-out, and smearing.

Keywords (TiC_p+TiB_w)/Ti–6Al–4V composites · Vitrified CBN wheel · Conventional speed grinding · Super-high speed grinding

1 Introduction

As is well known, titanium and its alloys offer superior properties, such as high strength-to-weight ratio, high toughness, super corrosion and creep resistance, and biocompatibility over a wide range of operating conditions, making them an attractive option in replacing some conventional materials in aerospace industry and increasing biomedical applications [1]. However, due to its poor tribological properties, high manufacturing process cost, and extreme affinity in molten state, the advanced materials are adopted in limited area under severe friction and wear conditions.

Under such condition, particle-reinforced titanium matrix composites are more desirable compared to titanium and its alloys owing to relative low manufacturing cost and isotropic property.

On the other hand, the particle-reinforced titanium matrix composites, i.e., (TiC_p+TiB_w)/Ti–6Al–4V composites (PTMCs for short), are relatively new, potentially useful structural materials with high ductility, high temperature property, good wear, and oxidation resistance. All of the above make it a more attractive alternative to titanium alloy and even nickel superalloy in fabricating the critical structural components and products. However, the nonhomogeneous and different mechanical properties between the reinforcements (that is, TiC particles and TiB whiskers) and Ti–6Al–4V matrix material make it a new type of difficult-to-cut material. Particularly, it is difficult to control the quality of the machined surface due to the high hardness and high brittleness of the reinforcements. Little research on the machining method and mechanism has been done for (TiC_p+TiB_w)/Ti–6Al–4V composites in recent years.

Grinding is an important method to machine difficult-to-cut material [2, 3]. The objective of this investigation is to study the grinding behavior of PTMCs. The comparative results are obtained using vitrified CBN grinding wheel at different wheel speeds, i.e., 20 m/s for conventional speed grinding and 120 m/s for super-high speed grinding. The grinding force and force ratio, the specific grinding energy, and the ground surface morphology are discussed.

In theory, compared to the conventional speed grinding, super-high speed grinding could offer the excellent potential for obtaining greater machining quality combined with high productivity [4, 5]. Additionally, in the super-high speed grinding process, the maximum chip thickness and the

B. Zhao · W. F. Ding (✉) · J. B. Dai · X. X. Xi · J. H. Xu
College of Mechanical and Electrical Engineering, Nanjing University of Aeronautics and Astronautics,
Nanjing 210016, Jiangsu, People's Republic of China
e-mail: dingwf2000@vip.163.com

grinding force may be decreased. Even the brittle material is expected to be removed in the mode of ductile flow. However, it is impossible to avoid completely the brittle fracture of the reinforcements during grinding PTMCs [6–8]. Therefore, in the present investigation, the grinding parameters are optimized to avoid the brittle fracture of the reinforcements to the greatest extent in order to achieve the precision surface of PTMCs.

2 Experimental details

The workpiece material (PTMCs), which is produced in the State Key Laboratory of Metal Matrix Composites of China, contains 10 vol.% (TiC_p+TiB_w) reinforcements and Ti–6Al–4V metal matrix. As a well-known way to fabricate PTMCs, the in situ method has been used to produce the (TiC_p+TiB_w)/Ti–6Al–4V composites. That is, the reinforcements are formed by in situ reactions between the reactants and the Ti–6Al–4V metal matrix in the molten state [9]. The following image about metallographic microstructure of the polished and etched samples is analyzed using a scanning electron microscope (SEM, Hitachi S-3400) showing the spherical and needle shapes, namely TiC particles and TiB whiskers (see Fig. 1). The composition and mechanical properties of PTMCs are listed in Table 1.

Figure 2 illustrates the setup of the grinding experiment [10]. The grinding force was measured with a piezoelectric dynamometer (Kistler 9272). The grinding temperature was detected by means of the thermocouple technique. Table 2 provides the experimental conditions.

3 Results and discussion

3.1 Grinding force and force ratio of PTMCs

The grinding force, that is the normal force and tangential one, has strong influence on the removal modes of the reinforcements and the matrix of PTMCs during grinding [11, 12]. The comparative research on the grinding force was carried out under the machining conditions of the wheel speed of 20 m/s and 120 m/s, respectively, as displayed in Fig. 3. Here the workpiece speed is fixed at 6 m/min, and the depth of cut is ranged from 0.005 mm to 0.020 mm.

As can be seen from Fig. 3a, the grinding force increases with an increase in workpiece speed and depth of cut. The normal force is 21.19 N and 9.88 N for the conventional speed grinding and super-high speed grinding, respectively, when the depth of cut is 0.005 mm, and the workpiece speed is fixed at 6 m/min. The tangential force is 9.46 N for the conventional speed grinding and 4.82 N for the super-high speed grinding, respectively. However, when the depth of cut is increased

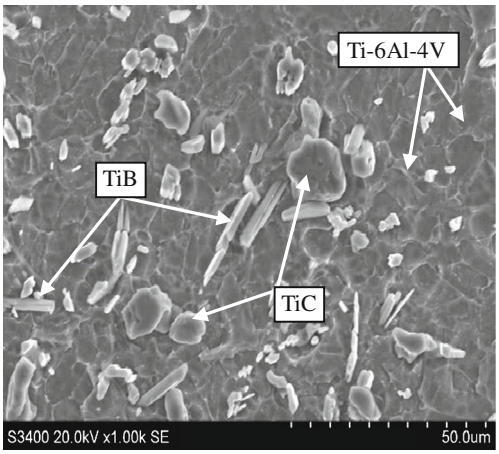

Fig. 1 Microstructure of (TiCp+TiBw)/Ti–6Al–4V composites (PTMCs for short)

from 0.005 mm to 0.020 mm, the normal force is increased rapidly by 340 % and 330 % to 71.46 N and 32.37 N for the conventional and super-high speed grinding, respectively. The tangential force is raised by 300 % and 240 % to 28.28 N and 11.52 N.

On the other hand, when the workpiece speed is ranged from 3 m/min to 12 m/min, it is found from Fig. 3b that the normal force is increased remarkably by 260 % from 24 N to 61 N in the conventional speed grinding process. However, the normal force is ranged from 17 N to 37 N, which is increased by about 220 % in the super-high speed grinding process. Meanwhile, the recorded tangential force is also increased approximately by 260 % from 10 N to 26 N in the conventional speed grinding process and by about 220 % from 5 N to 11 N in the super-high speed grinding process.

According to Fig. 3a, b, the magnitude of grinding force at the conventional wheel speed of 20 m/s is almost twice larger than that at the super-high wheel speed of 120 m/s. As can be seen from Fig. 4a, when the workpiece speed is 6 m/min, and

Table 1 Composition and mechanical properties of PTMCs

Types	Contents
Matrix	Ti–6Al–4V
Reinforcements	10 vol.% (TiC particles and TiB whiskers)
Dimensions of workpiece	30 mm (length)×25 mm (width)×5 mm (height)
Dimensions of reinforcements	TiC particle diameter: 1.5–10 μm TiB whisker length: 35–50 μm
Tensile strength	1102 MPa
Yield strength	972 MPa
Elongation rate	0.55 %
Elasticity modulus	133 MPa
Poisson's ratio	0.34

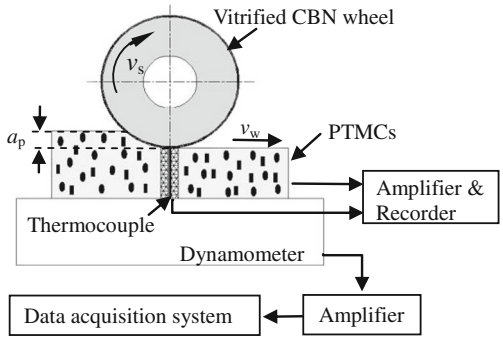

Fig. 2 Illustration of experimental setup for grinding

the depth of cut is between 0.005 mm and 0.020 mm, the force ratio of F_n versus F_t is in the range of 2.1–2.8 at the super-high wheel speed of 120 m/s. However, the generally smaller value of force ratio, 2.2–2.5, is achieved at the conventional wheel speed of 20 m/s. Meanwhile, the force ratio of F_n versus F_t, i.e., 2.12 to 2.39, at the conventional wheel speed of 20 m/s is remarkably lower than that, i.e., 3.18 to 3.63, at the super-high wheel speed of 120 m/s, as shown in Fig. 4b. Here, the depth of cut is fixed at 0.010 mm, and the workpiece speed is ranged from 3 m/min to 6 m/min. Higher force ratio always corresponds to severe tool wear; therefore, low tool sharpness in the super-high speed grinding process [13].

3.2 Grinding temperature of PTMCs

The grinding temperature was measured to determine the grinding state and optimize the grinding parameters [14]. As can be seen from Fig. 5, the greater depth of cut and the faster workpiece speed always result in the increase of the grinding temperature in the current investigation. According to Fig. 5a, when the depth of cut a_p is ranged from 0.005 mm to 0.020 mm, the grinding temperature are increased remarkably from 114 to 460 for the conventional speed grinding of 20 m/s and 562 to 659 for the super-high speed grinding of 120 m/s, respectively. When the workpiece speed v_w is varied between 3 m/min and 12 m/min, the grinding temperature is ranged

Table 2 Conditions for the grinding tests

Types	Contents
Machine tool	Ultra-high-speed precision surface grinding machine modeled BLOHM PROFIMAT MT-408
Abrasive wheel	Vitrified CBN wheel
Grinding mode	Up-grinding
Wheel speed v_s	20 and 120 m/s
Workpiece speed v_w	3–12 m/min
Depth of cut a_p	0.005–0.020 mm
Cooling fluid	Emulsified liquid; 5 % Dilution; 90 L/min; Pressure at 0.4 MPa

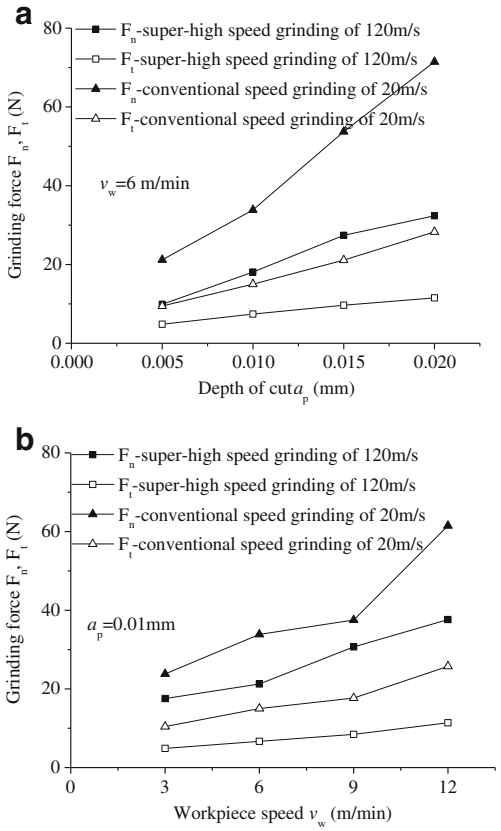

Fig. 3 Influence of grinding parameters on grinding force: (**a**) depth of cut; (**b**) workpiece speed

from 438 °C to 675 °C during super-high speed grinding and from 165 °C to 495 °C during conventional speed grinding, respectively, as shown in Fig. 5b. Obviously, the grinding temperature in the super-high speed grinding process of 120 m/s is always higher than that in the conventional speed grinding process of 20 m/s. The main reason is that the cooling fluid cannot enter the machining region due to the air barrier around the grinding wheel in the super-high speed grinding process. Therefore, sufficient cooling liquid with high pressure should be provided in order to control the grinding temperature in the further investigation.

The significant amount of heat generated in the grinding process can result in an undesirable change of the surface integrity of PTMCs. In particular, the increased grinding temperature usually leads to the color change of the machined surface. Fig. 6a, b provides the different ground surface, when the depth of cut is 0.005 mm and 0.010 mm, respectively. Here the workpiece speed is 6 m/min, and the wheel speed is 120 m/s. Obviously, the color of the machined zone in Fig. 6b has been greatly changed compared to that in Fig. 6a. Accordingly, it is known that a precision surface could be obtained when the depth of cut is 0.005 mm, and the workpiece speed is 6 m/min in the super-high speed grinding process.

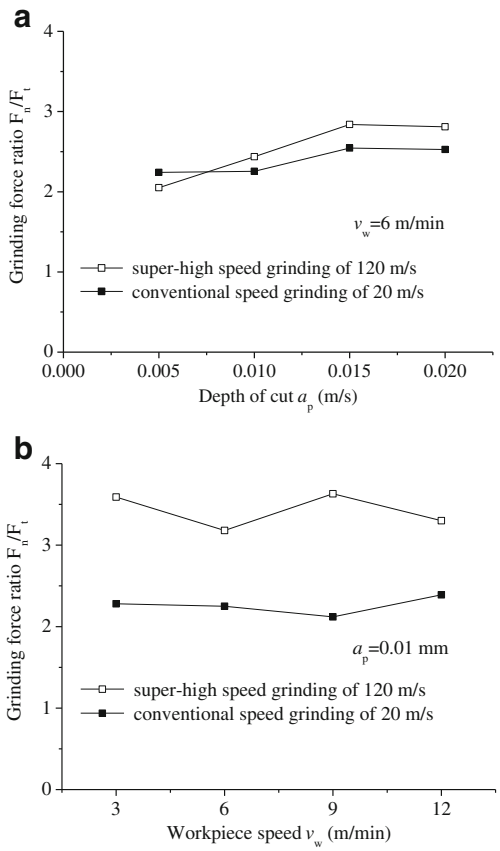

Fig. 4 Influence of grinding parameters on force ratio: (**a**) depth of cut; (**b**) workpiece speed

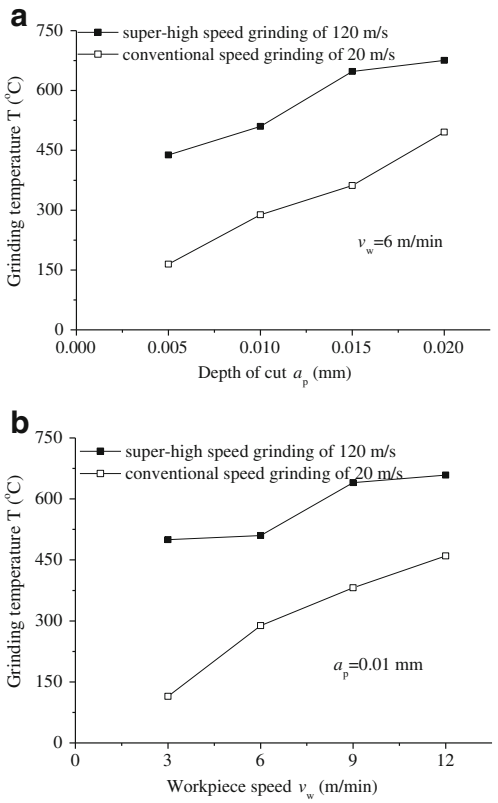

Fig. 5 Influence of grinding parameters on grinding temperature; (**a**) depth of cut; (**b**) workpiece speed

3.3 Specific grinding energy of PTMCs

The specific grinding energy, e_s, is an important grindability indicator. It can be written as [13]

$$e_s = \frac{F_t v_s}{v_w a_p b} \tag{1}$$

where b is the width of the grinding zone, i.e., 5 mm in this investigation.

On the other hand, the maximum undeformed chip thickness ($a_{g,max}$ for short) of the vitrified CBN wheel is represented by [15, 16]

$$a_{gmax} = \left(\frac{4v_w}{v_s N_d C}\sqrt{\frac{a_p}{d_s}}\right)^{1/2} \tag{2}$$

where N_d is the active cutting point density (8 mm^{-2} in this study), C=4tg θ (θ is a half of the angle of abrasive tip) is a constant correlated with the angle of the grain tip. d_s is the diameter of the grinding wheel, v_s is the wheel speed, and a_p is the depth of cut.

The specific grinding energy is obtained and plotted against the undeformed chip thickness, as presented in Fig. 7. This image indicates that the specific grinding energy is gradually decreased with the increase of the undeformed chip thickness [17]. According to Fig. 7, when the workpiece speed is 6 m/min, and the depth of cut is 0.010 mm, the specific grinding energy is high up to 160 J/mm^3 during super-high speed grinding of 120 m/s, which is remarkably higher than the specific grinding energy, i.e., 100 J/mm^3,

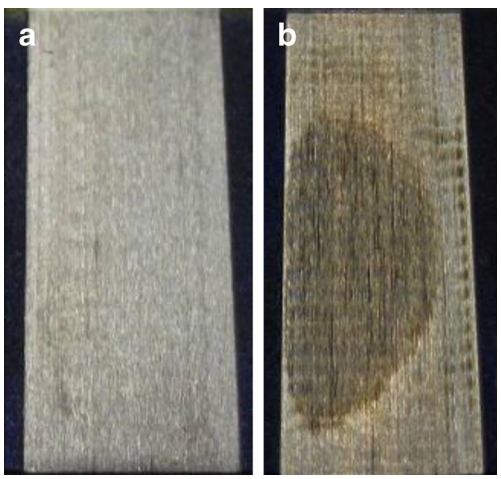

Fig. 6 Different colors of the ground PTMC surface; (**a**) color unchanged; (**b**) color changed

during conventional speed grinding of 20 m/s. The phenomenon can be explained from the viewpoint of the abrasive–workpiece interface. In the case of small undeformed chip thickness, the high specific grinding energy of PTMCs is mainly attributed to the high plowing and sliding energies, which are expended in excess of energy of chip formation during super-high speed grinding. When the undeformed chip thickness is increased, the energy contributed from plowing and sliding decreases. Under such condition, the specific grinding energy decreases with the increase of the undeformed chip thickness.

3.4 Ground surface morphology of PTMCs

The surface roughness of a ground component plays a significant role for fatigue endurance and corrosion resistance. In this investigation, the maximum surface roughness (R_{max} for short) was chosen and measured rather than the average surface roughness (R_a for short) [18]. The reason is that R_a may give misleading results on the machined surface including the fine grooves and micro-cracks [19]. The results reveal that the R_{max} value is varied in the range of 0.6–0.8 μm when the wheel speed is changed between 20 m/s and 120 m/s in the current investigation.

A high-quality ground surface region is demonstrated in Fig. 8, which is obtained in the super-high speed grinding of 120 m/s. Here the workpiece speed is 6 m/min, and the depth of cut is 0.005 mm. Under such condition, the reinforcements (including the TiC particles and TiB whiskers) and the matrix material are removed mainly in the ductile mode (see Fig. 8).

Meanwhile, the micrographs of the defects in the ground surface of PTMCs are displayed in Figs. 9a and d, respectively. All these images are detected with a scanning electron microscope (SEM) in a secondary mode during super-high speed grinding of 120 m/s. Here the workpiece speed is 6 m/min, and the depth of cut is 0.01 mm. In general, the defects produced in the ground surface region can be classified as: (a) voids and micro-cracks, (b) fracture or crushed, (c) pulled-out,

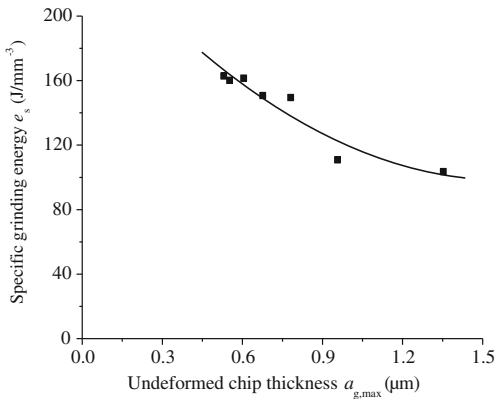

Fig. 7 Relationship between specific grinding energy and undeformed chip thickness

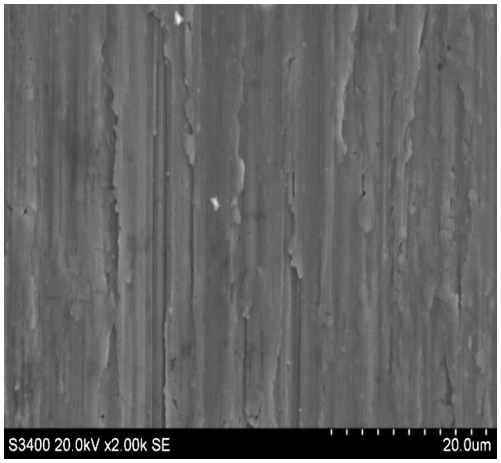

Fig. 8 Precision ground surface of PTMCs

and (d) smearing (see Fig. 9). The schematic image of the grinding process is given in Fig. 10, which briefly shows the several defects mentioned above [17, 19, 20].

As can be seen from Fig. 9a, the void was initiated obviously around the reinforcements (including the TiC particles and TiB whiskers) along the shear bonds on the machined surface. The phenomenon results from the dislocation pile-ups near the ground surface region and the debonding produced by the plowing of the hard reinforcements through the matrix surface during grinding operation [21]. Meanwhile, the presence of micro-cracks initiates at the surface due to the fracture and pullout of reinforcements with the increasing dislocation density and stress around the reinforcements. Some of those micro-cracks would extend into the Ti–6Al–4V metal matrix, and hence, the micro-cracks were presented on the machined surface (Fig. 9a), which would make the fatigue life of the material decrease substantially. It is observed from Fig. 9b that the reinforcements fractured or crushed due to the severe frictional and wear behavior by reducing the tendency for brittle fracture [22]. Some holes on the ground surface region are emerged, as displayed in Fig. 9c. The pullout behavior of the reinforcements was partially or totally detached from the machined surface and left behind cavities of various sizes and shapes due to the decohesion between the reinforcements and the Ti–6Al–4V matrix. Fig. 9d indicates the existence of long grooves parallel to the direction of the grinding velocity on the machined surface. These grooves were attributed to the reinforcements being pulled out from the matrix and becoming dragged along the surface for a distance and hence resulted in scratches of various lengths [23]. At the same time, the smearing on the machined surface took place owing to the fact that the machined surface was covered with the residual chips and the molten matrix. In particular, the residual chips were formed because they are not excluded completely in molten state during grinding. Meanwhile, the molten matrix was formed due to the redistribution and cooling on the ground surface under the high grinding temperature [24].

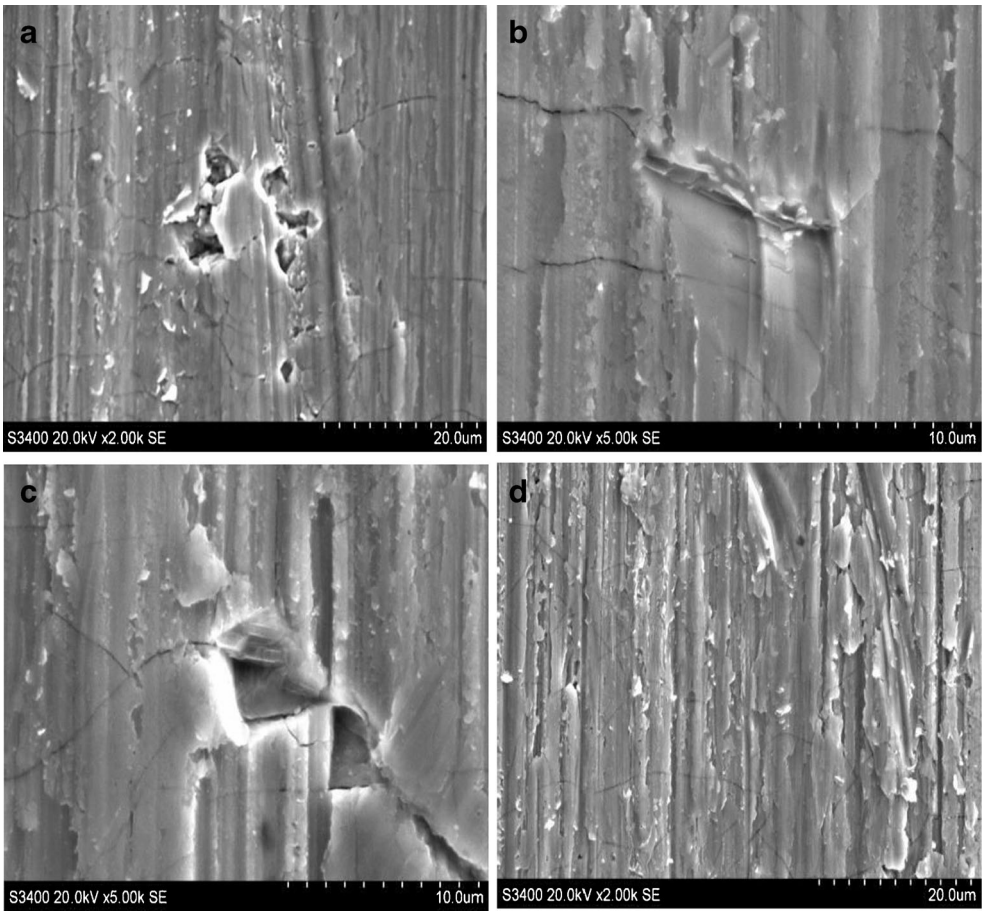

Fig. 9 Main defects of the ground PTMCs surface: (**a**) voids and micro-cracks; (**b**) fracture or crushed; (**c**) pulled-out; (**d**) smearing

It is noted that the defect patterns of the PTMC surface produced during conventional speed grinding of 20 m/s are generally similar to that during super-high speed grinding of 120 m/s. However, the proportion of surface defect patterns induced by means of different removal behaviors of reinforcements is changed with the wheel speed during grinding. For instance, in the grinding process of PTMCs, the reinforcements (including the TiC particles and TiB whiskers) always tend to prevent the titanium alloy matrix from plastic deformation. When the wheel speed is high, more voids around the reinforcements are produced, and the reinforcements become fracture or crushed, as shown in Fig. 9a. The phenomenon is attributed to the higher strain rate of the matrix compared to that of the brittle reinforcements in the grinding process. The debonding of reinforcements is favorable to emerge in the conventional speed grinding process because of higher grinding force. In particular, the approximate proportion of the defects of the ground surface in the conventional speed grinding process and in the super-high speed grinding process, respectively, will be discussed in the further investigation.

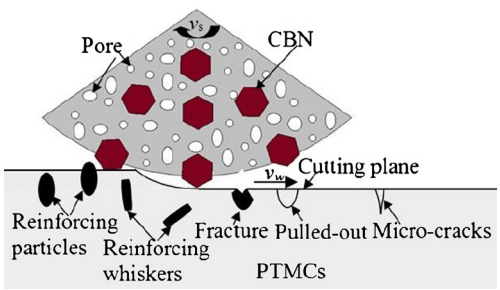

Fig. 10 Schematic image of the defects of the ground PTMCs surface

4 Conclusions

(1) Under the identical condition, the normal force F_n and the tangential force F_t obtained at the super-high wheel speed of 120 m/s are smaller than that at the conventional wheel speed of 20 m/s during grinding PTMCs. However, the force ratio of F_n/F_t at the wheel speed of 120 m/s is always much larger than that at the wheel speed of 20 m/s.

(2) The grinding temperature and specific grinding energy of PTMCs during super-high speed grinding is greater than that during conventional speed grinding. Precision surface is obtained in the super-high speed grinding process of 120 m/s when the depth of cut is 0.005 mm, and the workpiece speed is 6 m/min. Here, the grinding temperature is below 450 °C.

(3) The main defects of the ground PTMC surface are voids and micro-cracks, fracture or crushed, pulled-out, and smearing. However, the defect proportion induced by means of different removal patterns of the reinforcements in the conventional speed grinding process is different from that in the super-high speed grinding process.

Acknowledgments The authors gratefully acknowledge the financial support of the Fundamental Research Funds for the Central Universities (No. NS2013051) in this research.

References

1. Teicher U, Kunanz K, Ghosh A (2008) Performance of diamond and CBN single-layered grinding wheels in grinding titanium. Mater Manuf Process 23:224–227
2. Kim JS, Lee KM, Cho DH, Lee YZ (2012) Fretting wear characteristics of titanium matrix composites reinforced by titanium boride and titanium carbide particulates. J Mater Sci 301:562–568
3. Ezugwu EO (2005) Key improvements in the machining of difficult-to-cut aero-space superalloys. Int J Mach Tool Manuf 45:1353–1367
4. Ranganath S (1997) A review on particulate-reinforced titanium matrix composites. J Mater Sci 32:1–16
5. Kim IY, Choi BJ, Kim YJ, Lee YZ (2011) Friction and wear behavior of titanium matrix (TiB+TiC) composites. Wear 271:1962–1965
6. Jackson MJ, Davis CJ, Hitchiner MP, Mills B (2001) High-speed grinding with CBN grinding wheels—applications and future technology. J Mater Process Technol 110:78–88
7. Kopac J, Krajnik P (2006) High-performance grinding—a review. J Mater Process Technol 175:278–284
8. Qu NS, Xu ZY (2013) Improving machining accuracy of electrochemical machining blade by optimization of cathode feeding directions. Int J Adv Manuf Technol 68:1565–1572
9. Huang LJ, Geng L, Peng HX (2010) In situ (TiB_w+TiC_p)/Ti6Al4V composites with a network reinforcement distribution. Mater Sci Eng A 527:6723–6727
10. Mao C, Zhou ZX, Zhang J, Huang XM, Gu DY (2011) An experimental investigation of affected layers formed in grinding of AISI 52100 steel. Int J Adv Manuf Technol 54:515–523
11. Shi Z, Malkin S (2006) Wear of electroplated CBN grinding wheels. J Manuf Sci Eng 128:110–118
12. Li ZC, Lin B, Xu YS, Hu J (2002) Experimental studies on grinding forces and force ratio of the unsteady-state grinding technique. J Mater Process Technol 129:76–80
13. Hwang TW, Malkin S (1999) Upper bond analysis for specific energy in grinding of ceramics. Wear 231:161–171
14. Xu XP, Malkin S (2001) Comparison of methods to measure grinding temperature. J Manuf Sci Eng 123(2):191–195
15. Ghosh S, Chattopadhyay AB, Paul S (2008) Modelling of specific energy requirement during high-efficiency deep grinding. Int J Mach Tool Manuf 48(11):1242–1253
16. Ren YH, Zhang B, Zhou ZX (2009) Specific energy in grinding of tungsten carbides of various sizes. Annals of the CIRP 58:299–302
17. Xu XP, Li Y, Malkin S (2001) Forces and energy in circular sawing and grinding of granite. J Manuf Sci Eng 123:13–22
18. Yan L, Rong YM, Jiang F, Zhou ZX (2011) Three-dimension surface characterization of grinding wheel using white light interferometer. Int J Adv Manuf Technol 55:133–141
19. Hocheng H, Yen SB, Ishihara T, Yen BK (1997) Fundamental turning characteristics of a tribology-favored graphite/aluminum alloy composite material. Compos Part A 28:883–890
20. Zhong ZW, Hung NP (2000) Diamond turning and grinding of aluminum-based metal matrix composites. Mater Manuf Process 15(6):853–865
21. Schubert A, Nestler A (2011) Enhancement of surface integrity in turning of particle reinforced aluminium matrix composites by tool design. Procedia Engineering 19:300–305
22. Ulutan D, Ozel T (2011) Machining induced surface integrity in titanium and nickel alloys: a review. Int J Mach Tool Manuf 51: 250–280
23. El-Gallab M, Sklad M (1998) Machining of Al:SiC particulate metal matrix composites: part II: workpiece surface integrity. J Mater Process Technol 83:277–285
24. Rech J, Moisan A (2003) Surface integrity in finish hard turning of case-hardened steels. International Journal of Machine Tools & Manufacture 43:543–550